19 July 1985, Volume 229, Number 4710

SCIENCE

Pentagonal and Icosahedral Order in Rapidly Cooled Metals

David R. Nelson and Bertrand I. Halperin

Summary. The discovery of an alloy of aluminum and manganese with sharp Bragg diffraction spots and an icosahedral point group symmetry was announced last year. The icosahedral symmetry appears to be an intrinsic property of the material and not an artifact of twinning. There are remarkable similarities between the observed diffraction patterns and aperiodic tesselations of space called Penrose tiles. The relation between the experiments and Penrose tiles, as well as phenomenological descriptions of the icosahedral aluminum-manganese alloy as a superposition of incommensurate density waves, are reviewed. Other types of exotic crystallography are also discussed.

One of the most remarkable discoveries in the history of crystallography was announced last year, when Shechtman and colleagues observed tenfold symmetry axes in patterns of Bragg diffraction spots from a rapidly cooled alloy of aluminum and manganese (*1*). A theorem of classical crystallography states that five- or tenfold symmetry axes can never appear in a truly periodic crystal—that is, one constructed from a single unit cell that repeats indefinitely in space. Spurious Bragg patterns with tenfold symmetry can be produced through macroscopic twinning of an ordinary crystal; such spurious patterns have been seen, for example, in small gold particles (*2*). The experiments of Shechtman *et al.*, however, clearly indicate that the tenfold symmetry pattern in the aluminum-manganese alloy is an intrinsic property, reflecting the fundamental microscopic arrangement of atoms in the material. Needless to say, there is currently great excitement in this field as experimentalists and theorists try to understand and explain this new structure.

At present, there is no published theory of these alloys that is satisfactory in all details. There are, however, mathematical models that have many features in common with the observed diffraction patterns. We shall review some of these mathematical models and discuss their relation to the new phase of aluminum-manganese. We shall also discuss some other materials with nonstandard diffraction patterns that have been discovered in recent years.

The Icosahedral Phase of Aluminum-Manganese

The full point symmetry group of the experimentally observed diffraction pattern of this alloy corresponds to a Platonic solid called the icosahedron (see Fig. 1). The icosahedron has six fivefold symmetry axes, which can be detected by bringing a sample of the new icosahedral phase of Al-Mn into the proper orientation. There are 10 threefold and 15 twofold symmetry axes as well. The samples are made by rapidly cooling an aluminum-rich liquid with approximately 14 atom-percent manganese; some variation in the amount of manganese is possible, and manganese can be replaced by other transition metals. The molten alloy is quenched on a rapidly rotating metal wheel, which leads to cooling rates of the order of 10^6 degrees per second. Such large cooling rates are necessary to avoid nucleating a conventional crystal such as Al_6Mn, which has a 28-atom orthorhombic unit cell. This same melt-spinning technique is often used to prepare amorphous metal alloys (*3*); part of the excitement surrounding the discovery of the icosahedral phase is the insight it may provide into the structure of metallic glasses.

A transmission electron diffraction pattern from the icosahedral phase of $Al_{0.86}Mn_{0.14}$ in a plane normal to a fivefold symmetry axis (*4*) is shown in Fig. 2. Because any structure factor must have inversion symmetry, the underlying fivefold axis shows up as an array of Bragg spots with a tenfold symmetry. The angular modulation of the diffraction pattern shows that the orientations of icosahedral packing units in the material are correlated over a distance at least as large as the illumination volume of the diffracted beam, which is typically 10^4 to 10^5 Å. Each spot in the diffraction pattern corresponds to a set of Bragg planes, and we can also ask about the extent of the translational order embodied in these density waves. The spots are fairly sharp, suggesting a translational correlation length of a few hundred angstroms. Many samples have frozen-in strains, however, and this correlation length might be much larger in strain-free specimens. There is no known reason, in principle, why the peaks could not be infinitely sharp, just as in conventional crystals.

It is possible to simulate an erroneous icosahedral diffraction pattern by using particle clusters with an overall icosahedral shape but with conventional local crystalline order. The well-known "cannonball" stacking of hard spheres, for example, can be used to make tetrahedral fragments of a perfect *fcc* crystal. Twenty such tetrahedra can be combined, with distortions, to make an icosahedron (*2*). The (111) faces of the distorted tetrahedra meet at twin bound-

---

The authors are at the Lyman Laboratory of Physics, Harvard University, Cambridge, Massachusetts 02138.

aries. An explanation such as this has been proposed for the icosahedral phase of Al-Mn (*5*). Shechtman *et al.*, however, presented several pieces of evidence that appear convincingly to rule out the twinning interpretation (*1*); even more unambiguous evidence against this hypothesis is provided by lattice-imaging experiments that have been carried out in a number of different laboratories (*6*). When the sample is viewed along a fivefold symmetry axis, the five coexisting sets of atomic planes with normals pointing to the vertices of a regular decagon can actually be seen. In the best samples, the planes in each set are perfectly parallel, and the pattern extends over distances of several thousand angstroms. The icosahedral order in Al-Mn is an intrinsic property and not an artifact of twinning.

Penrose Tiles

Independent of these experimental developments, mathematicians and some physicists had been exploring the consequences of the discovery by Penrose in 1974 of some remarkable, aperiodic, two-dimensional tilings with fivefold symmetry (*7*). Several authors suggested that these unusual tesselations of space might have some relevance to real materials (*8, 9*). MacKay (*8*) optically Fourier-transformed a two-dimensional Penrose pattern and found a tenfold symmetric diffraction pattern not unlike that shown for Al-Mn in Fig. 2. Three-dimensional generalizations of the Penrose patterns, based on the icosahedron, have been proposed (*8–10*). The generalization that appears to be most closely related to the experiments on Al-Mn was discovered by Kramer and Neri (*11*) and, independently, by Levine and Steinhardt (*12*), who had been carrying out their own investigation of Penrose patterns starting in 1982. Levine and Steinhardt were able to Fourier-transform a simplified version of this three-dimensional Penrose pattern and to show that it had δ-function Bragg peaks. In the planes perpendicular to the fivefold and threefold axes, the positions of the most intense Bragg peaks of the model agreed with the experimentally observed spot positions of Al-Mn after adjustment of the arbitrary lattice constant of the model. (The agreement was not so good, however, for the simplified model in planes normal to the twofold axis.)

Penrose patterns are constructions in which an infinite Euclidean space is filled with an admixture of two distinct unit cells. Each type of unit cell can be imagined as being occupied by a fixed arrangement of atoms, just as in conventional crystal lattices. It is the existence of two unit cells, occurring in an irrational proportion, that allows deviations from the rules of classical crystallography, which assume that a single unit cell is repeated periodically in space. Nevertheless, the requirement that space be completely filled imposes rigid constraints on the allowable Penrose patterns. This in turn has strong implications for the diffraction pattern, or Fourier transform, of the structure.

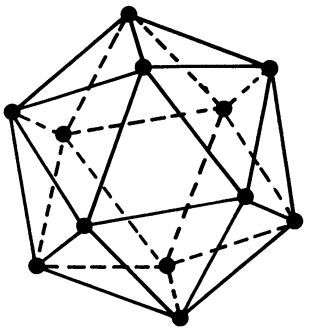

Fig. 1. The icosahedron. Six fivefold symmetry axes pass through the 12 vertices. The three- and twofold symmetry axes are associated with the 20 faces and 30 edges, respectively.

These ideas can be illustrated most easily by a two-dimensional Penrose tiling [see (*13*)]. The basic building blocks are the "arrowed rhombuses" shown in Fig. 3. Both the thick and the thin rhombus have identical edge lengths, and all interior angles are integral multiples of 36°. A Penrose tiling is formed when these rhombuses are fit together so that the edges with single and double-headed arrows match (see Fig. 4). In an infinite Penrose tiling, the two rhombuses must occur in the ratio of the golden mean, $\tau = (\sqrt{5} + 1)/2$, with the larger tile being more prevalent (*7, 8*). Equivalent tilings, based on unit cells with the shapes of "kites" and "darts," are also possible (*7*).

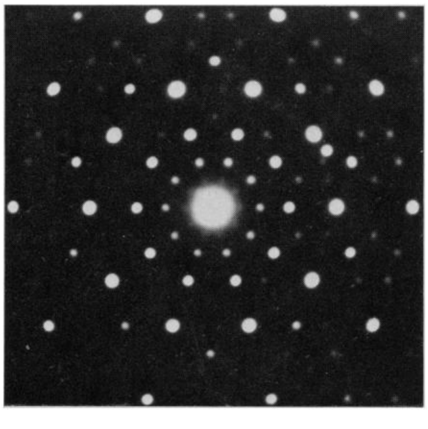

Fig. 2. Diffraction pattern normal to a fivefold symmetry axis in the icosahedral phase of Al-Mn (*4*).

Because all interior angles in the tiles are multiples of one-tenth of a complete rotation, all rhombus edges must point to the vertices of a regular decagon. A more sophisticated analysis shows that the edges are equally distributed among the ten vertices (*13*). It follows immediately that there is tenfold, long-range orientational order in this system. This orientational order is illustrated in Fig. 4, where several different decagons with identical orientations are highlighted. The Fourier transform of any pattern of this kind is guaranteed to have a tenfold orientational modulation.

Penrose patterns also have a more subtle, translational symmetry that is responsible for the sharpness of the Bragg spots in the diffraction pattern. In Fig. 5, we have superimposed on a two-dimensional Penrose pattern a grating of parallel lines, separated by a distance d which corresponds to the wave vectors of one of the sharp diffraction peaks, according to the standard diffraction law, $\mathbf{q} = \pm (2\pi/d)\hat{\mathbf{n}}$, where $\hat{\mathbf{n}}$ is a unit vector normal to the grid lines. There is a one-to-one correspondence between these grid lines and rows of rhombuses, connected by a set of common parallel bonds, which are indicated by shading in Fig. 5. The shaded rows are typically displaced to one side or the other of the grid lines, but they remain close to the corresponding lines even for a sample of infinite size. This finite "wandering" of the rows will lead to a decrease in the intensity of the Bragg spots, associated with diffraction from the grid, but it will not cause broadening of the spot. In all, there are five families of parallel grid lines of spacing d, with normals pointing to the vertices of a regular decagon. De Bruijn's classification of the possible types of Penrose patterns (*13*) is based on the symmetries of these "pentagrids."

This construction suggests that the observed diffraction pattern will contain a "star" of ten sharp Bragg spots at reciprocal lattice vectors, whose values are given by Eq. 1.

$$\{\mathbf{G}_i = (2\pi/d)\hat{\mathbf{n}}_i;\ i = 1, \ldots, 10\} \qquad (1)$$

where the values for $\hat{\mathbf{n}}_i$ are unit vectors pointing to the vertices of a decagon. In a strongly interacting system, however, ordering with some periodicity will typically induce ordering at all "harmonics" of the basic period. Here, the "harmonic'' wave vectors are simply linear combinations of the basis set (Eq. 1) with positive integer coefficients. In ordinary crystals, this construction leads to a regular lattice of diffraction spots in reciprocal space. A peak belongs to the *m*th generation if *m* is the minimum number of elements of the basic star required to produce the wave vector of the peak. Figure 6 shows the first three generations of Bragg spots produced by the wave vectors in the basis set (Eq. 1). Figure 6 is remarkably similar to the experimentally observed diffraction pattern for Al-Mn shown in Fig. 2.

Unlike conventional crystals, the diffraction peaks of a Penrose pattern do not lie on a periodic lattice in reciprocal space. The crucial difference is the existence of two irrationally related length scales. As shown in Fig. 7, two elements of the tenfold basis set combine to give another basis vector multiplied by the golden mean. Because of this incommensurability, peaks can be generated arbitrarily close to any given position by taking increasingly complex linear combinations of the fundamental basis set. However, we might expect a decreasing hierarchy of peak intensities, depending on how many elements of the star were required to make a particular peak.

If we allow negative as well as positive integer coefficients, all reciprocal lattice peaks can be expressed as combinations of just five vectors pointing to the vertices on a pentagon in reciprocal space (see Fig. 7). Hence, it is convenient to use five ''Miller indices'' to specify a particular spot position. This observation makes plausible de Bruijn's result that the vertices of the two-dimensional Penrose tiling in real space are related to a projection of a five-dimensional, simple hypercubic lattice into two dimensions (*13*). Kramer and Neri (*11*) generalized de Bruijn's projection technique to produce a three-dimensional Penrose pattern. Here, the building blocks are fat and thin rhombohedra, again in the ratio of the golden mean. The interior solid angles of these rhombohedra are all integral multiples of one-twentieth of 4π. Elser and, independently, Duneau and Katz have devised an elegant technique for computing the diffraction pattern of a three-dimensional Penrose pattern, regarded as the projection of a six-dimensional hypercubic lattice (*14*). Like Levine and Steinhardt (*12*), they found δ-function peaks with an icosahedral symmetry in reciprocal space. In contrast to the simplified pattern studied by Levine and Steinhardt (*12*), there is now excellent agreement with the experimentally observed diffraction patterns normal to the twofold, as well as to the three- and fivefold, symmetry axes. The positions of the most intense twofold peaks scale with τ^{-1} in the Levine-Steinhardt diffraction pattern; these peaks scale with τ^{-3} in the experiments.

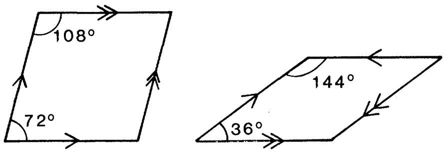

Fig. 3. Arrowed rhombuses, which are the building blocks of the two-dimensional Penrose patterns.

Structures containing several incommensurate spatial periodicities, which are not simply periodic but nevertheless have a diffraction pattern with δ-function Bragg peaks, might be called ''quasicrystals,'' by analogy with the term ''quasiperiodic motion'' that is used for simple dynamic systems having two incommensurate periods. We shall employ the term ''quasicrystal'' in this general sense below, although Levine and Steinhardt (*12*) imposed some additional restrictions in their definition.

Incommensurate Icosahedral Density Waves

As an alternative to a description such as the Penrose construction, which focuses on the positions of atoms in physical space, icosahedral quasicrystals can also be described in terms of the density of atoms, $\rho(\mathbf{r})$, or, more conveniently, in terms of the Fourier transform of the density, $\rho_{\mathbf{q}}$, in reciprocal space. This approach, which is based on Landau's description of conventional crystallization (*15*), has been applied to icosahedral crystals by a number of investigators (*16–19*).

We start by describing the free energy *F* of a liquid as a function of the deviation of the density $\rho(\mathbf{r})$ from its mean value ρ_0, as in Eq. 2.

$$F[\delta\rho(\mathbf{r})] = \frac{1}{2}\int d\mathbf{r}\int d\mathbf{r}'\, K(\mathbf{r}-\mathbf{r}')\delta\rho(\mathbf{r})\delta\rho(\mathbf{r}') + \int d\mathbf{r}[w(\delta\rho)^3 + u(\delta\rho)^4 + \ldots] \qquad (2)$$

where $\delta\rho(\mathbf{r}) = \rho(\mathbf{r}) - \rho_0$. The quadratic term is nonlocal and represents the effects of interactions in the liquid that promote ordering. The second term, which is local in our approximation, represents the nonlinearities that prevent $\rho(\mathbf{r})$ from deviating too far from its mean value in the ordered phase. In the liquid, we neglect these nonlinearities and find that the Fourier transform of the nonlocal kernel, $\hat{K}(\mathbf{q})$, is inversely proportional to the liquid structure factor, $S(\mathbf{q})$, which arises from thermal fluctuations in the density as given by Eq. 3.

$$S(\mathbf{q}) = <|\rho_{\mathbf{q}}|^2> = k_BT/\hat{K}(\mathbf{q}) \qquad (3)$$

where k_B is Boltzmann's constant and *T* is temperature (in kelvins).

To test for possible crystalline phases, we expand $\rho(\mathbf{r})$ in a discrete set of reciprocal lattice vectors $\{\mathbf{G}\}$ characterizing the crystal.

$$\rho(\mathbf{r}) = \rho_0 + \sum_{\mathbf{G}} \rho_{\mathbf{G}} e^{i\mathbf{G}\cdot\mathbf{r}} \qquad (4)$$

The free energy becomes

$$F = \frac{1}{2}\sum_{\mathbf{G}}\hat{K}(\mathbf{G})\,|\rho_{\vec{\mathbf{G}}}|^2 + w\sum_{\mathbf{G}_1+\mathbf{G}_2+\mathbf{G}_3=0}\rho_{\mathbf{G}_1}\rho_{\mathbf{G}_2}\rho_{\mathbf{G}_3} + u\sum_{\mathbf{G}_1+\mathbf{G}_2+\mathbf{G}_3+\mathbf{G}_4=0}\rho_{\mathbf{G}_1}\rho_{\mathbf{G}_2}\rho_{\mathbf{G}_3}\rho_{\mathbf{G}_4} + \ldots \qquad (5)$$

For a suitable choice of the signs and magnitudes of the coefficients and for a suitable choice of the function $\hat{K}(\mathbf{G})$, we can expect that the state of lowest free energy will be a reciprocal quasilattice with icosahedral symmetry or, in two dimensions, the tenfold symmetric pattern illustrated in Fig. 6. The Fourier components that are easiest to form will be those for which $\hat{K}(\mathbf{q})$ is smallest, corresponding to peaks in the structure factor. The nonlinearities in Eq. 5 lead to the ''harmonic'' reciprocal space peaks discussed above in the context of the Penrose tiles, and they lock together the phases of various Fourier components.

A hypothetical liquid structure factor that might lead to a two-dimensional ''crystal'' with the symmetry of the Penrose tiles is shown in Fig. 8. There is a sharp peak at q_0, which is the radius of the decagon of brightest spots in Fig. 6. The second generation of spots in Fig. 6 occurs at radii that are 0.618, 1.176, 1.618, 1.902, and 2.0 times q_0. We have made our structure factor large at these positions as well. Figure 8 is a rather unusual structure factor for a two-dimensional liquid, and consequently we would not expect two-dimensional pentagonal crystals to be very common.

In three dimensions, however, all the experimentally observed peaks in Al-Mn are combinations of reciprocal lattice vectors that point to the vertices of an icosahedron of radius q_0 (*17*). Now there are second generation peaks at distances 1.052, 1.701, and 2.0 times q_0. In alloys that form metallic glasses (*20*), the structure factor has one pronounced peak that is broad enough to accommodate ordering at both a fundamental wave vector q_0 and at 1.052 q_0. There is, in addition, a smaller peak at 1.7 q_0 and a shoulder at 2.0 q_0. These observations make the formation of three-dimensional icosahedral crystals from an undercooled liquid alloy somewhat less surprising.

Other Exotic Crystallographies

Quasicrystals with two incommensurate periodicities have actually been observed in the past. In 2H-$TaSe_2$, for example, there are one-dimensional charge density modulations superimposed on a conventional ionic lattice (*21*). The periodicity of the charge density wave is determined by the geometry of the Fermi surface and can, in general, be incommensurate with the underlying crystalline lattice. Krypton overlayers on a graphite substrate can form an incommensurate two-dimensional crystal whose lattice constant is a continuous function of temperature and pressure (*22*). There are three-dimensional incommensurate spin density waves in chromium (*23*). In all these systems, sharp diffraction peaks are expected at all wave vectors that are linear combinations of two sets of reciprocal lattice vectors with an irrational relationship.

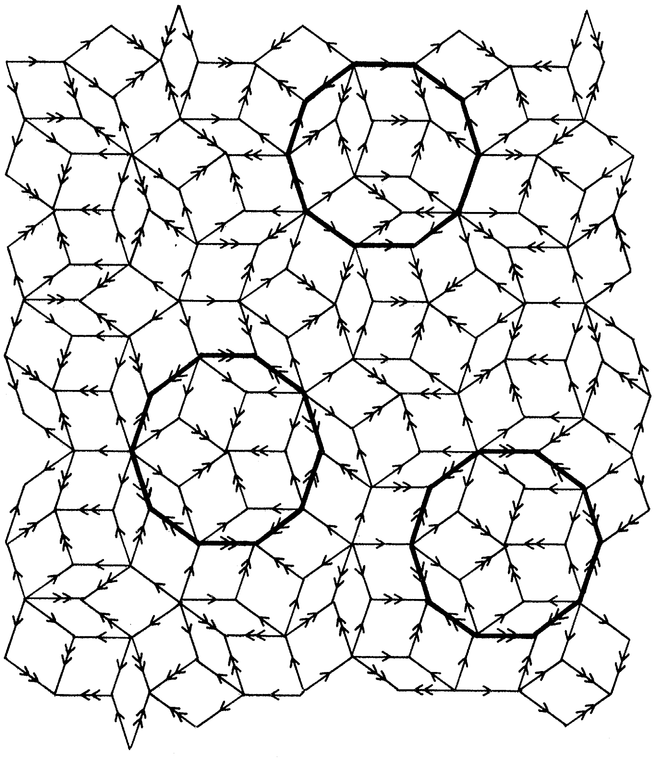

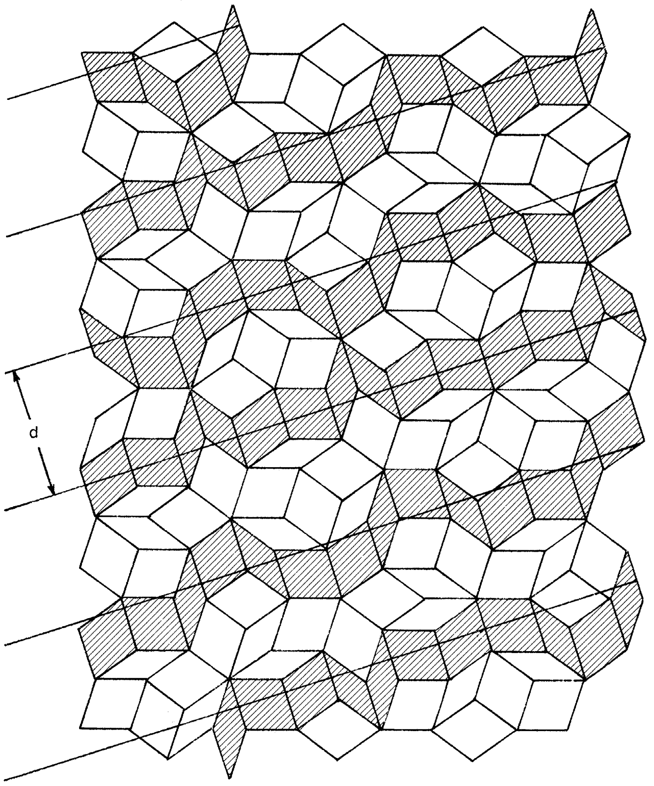

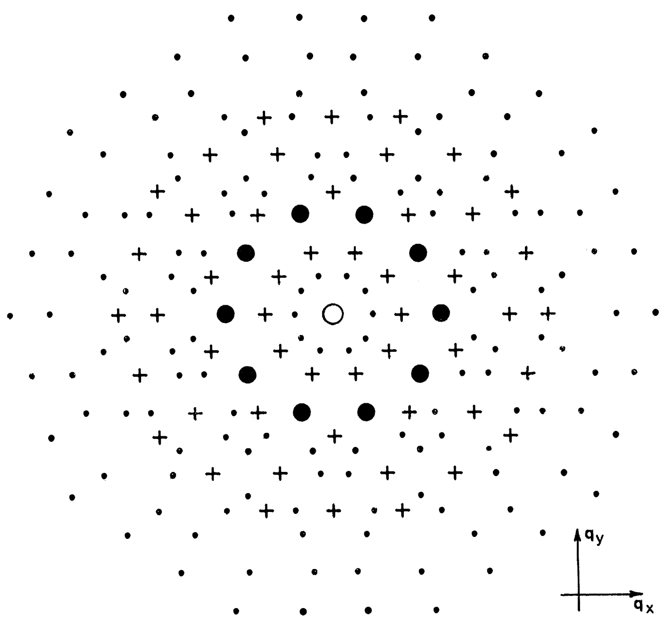

Fig. 4 (top left). Two-dimensional Penrose tiling, illustrating how the arrowed rhombuses (Fig. 3) fit together. Three decagons, all with the same orientation, are shown in boldface. All decagons contain five thick and five thin rhombuses. Fig. 5 (top right). A regularly spaced diffraction grid is superimposed on the Penrose pattern of Fig. 4. Each shaded row of tiles may be associated with a particular grid line. Four similar sets of grid lines with the same spacing *d* may be constructed at angles of 36° and 72° to the set shown. Fig. 6 (bottom right). First three generations of intensity maxima in reciprocal space for a two-dimensional Penrose tiling. Symbols: (●) first generation; (+) second generation; (•) third generation.

What distinguishes the new phase of Al-Mn from all previous systems is its icosahedral symmetry. A consequence of this symmetry is the locking of the incommensurate length scales in particular ratios, determined by geometry (see, for example, Fig. 7). In conventional incommensurate crystals, the ratio of periodicities is a continuous function of external parameters such as temperature or impurity concentration. The analogy between icosahedral Al-Mn and conventional incommensurate systems is clearly presented and exploited in the papers by Bak (*16*).

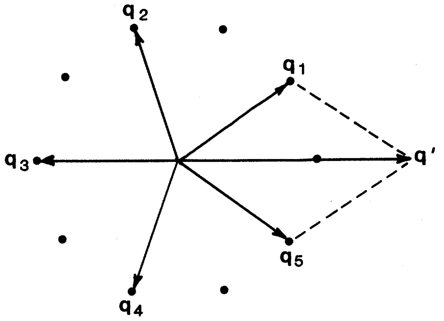

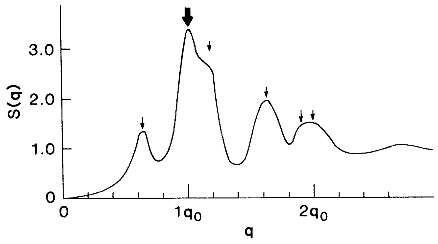

Fig. 7 (left) Decomposition of the decagon of brightest spots in Fig. 6 into a pentagonal set of five basis vectors. Two of these vectors can be combined to give a vector which is the negative of the golden mean times another element of the set: $\mathbf{q}' = \mathbf{q}_1 + \mathbf{q}_5 = -\frac{1}{2}(1 + \sqrt{5})\mathbf{q}_3$. Fig. 8 (right). Hypothetical liquid structure factor that might give rise to a two-dimensional Penrose crystal at low temperatures. The large arrow at q_0 corresponds to the radius of the primary peaks in Fig. 6. The radii of the second-generation peaks in Fig. 6 are marked by smaller arrows.

Another kind of exotic crystallography reflects the distinction between orientational and translational order. It is possible to imagine phases of matter with long-range order in the orientations of local crystallographic axes but with short-range translational order. A familiar example is the nematic liquid-crystal phase, in which rod-like molecules align themselves parallel to some chosen axis.

A more surprising example is the hexatic phase, which appears in theories of dislocation-mediated melting in two dimensions (*24*). Hexatics are liquids with extended correlations in the orientations of local hexagonal packing units. Bulk hexatic phases have been observed in certain smectic liquid crystals (*25*), in which molecules are stacked in two-dimensional liquid-like layers. In the hexatic phase, there is a sixfold modulation in the in-plane x-ray diffraction pattern, with intensity maxima at positions characteristic of a two-dimensional triangular lattice. The peaks of the hexatic are not sharp δ-functions, however. The translational correlation length, as measured by the inverse radial width of the Bragg spots, is finite and varies continuously with temperature. In the material 95SBC, translational correlation lengths roughly as large as 500 Å (about 100 molecular diameters) have been measured in the hexatic phase (*26*).

In two dimensions, it is natural to suppose that particles in a liquid will arrange themselves to form short-range hexagonal rather than pentagonal order. As pointed out by Frank (*27*), however, there are energetic reasons for the icosahedron to be preferred in three dimensions. In 1981, Steinhardt and co-workers studied icosahedral orientational order in a molecular dynamics simulation of an undercooled Lennard-Jones liquid (*28*). They observed icosahedral correlations that grew with undercooling and proposed an icosahedral analog of the hexatic phase. It is possible that the icosahedral phase of Al-Mn is a kinetically frozen version of such an icosahedral "liquid crystal," with a large but finite translational correlation length. The translational order would then be expected to be broken up by dislocations, in analogy to what happens in two-dimensional hexatics (*24*). Few dislocations appear in lattice images (*4*), however, so that the icosahedral liquid crystal interpretation appears to be an unlikely one for Al-Mn. The finite translational correlation lengths observed experimentally (*29*) are probably due to frozen-in strains.

Open Questions

Although models based on the Penrose tiles properly account for the peak positions in the Al-Mn diffraction patterns, we do not yet have a good understanding of the peak intensities. Knowing the intensities amounts to knowing how the aluminum and manganese atoms are distributed in the two rhombohedral unit cells. Icosahedral crystals form over a composition range of about 10 to 25 atom-percent manganese, which further complicates the issue. We would also like to know what energetics favor formation of these cells. Can we predict in advance which alloys would be likely to form an icosahedral phase? How do these materials grow?

Other questions concern defects. We might, for example, try to make an edge dislocation by removing a half-row of shaded rhombuses in Fig. 5. Although the remaining tiles fit neatly together, the arrows on the edges of the rhombuses no longer match (see Fig. 4). If there are forces corresponding to these arrows, edge dislocations formed in this way will be partials, connected by a stacking fault. Levine and colleagues have constructed a hydrodynamic theory of icosahedral crystals (*18*) and have found that dislocations are possible but that they must be characterized by six-index Burgers vectors. It is convenient to use five-index Burgers vectors in two dimensions. Unlike ordinary dislocations, these defects involve rearrangements of particles at arbitrary distances from the dislocation core. It is not yet known whether these defects will occur naturally in a growing crystal, and, once present, whether they will be able to move under deformation.

The cooling techniques employed to make icosahedral Al-Mn are commonly used to fabricate metallic glasses. It will be interesting to see whether icosahedral Al-Mn can be reconciled with our understanding of these systems. If the alloy is cooled very rapidly, the icosahedral crystal can be bypassed and an Al-Mn glass can be made (*30*). Many metallic glasses are believed to contain short-range icosahedral order, broken up by wedge disclination lines (*31*). This order is conveniently measured with respect to an ideal icosahedral template (called polytope {3,3,5}), which is only defect-free when embedded in the curved surface of a four-dimensional sphere. A good description of the structure factor of glassy metals can be obtained by use of this approach (*32*). The ground states in these theories are ordered arrays of disclination lines. The Frank-Kasper phases of transition metal alloys, which contain many icosahedra, are common examples. It is also possible to construct an aperiodic Frank-Kasper phase with long-range icosahedral order, notwithstanding the presence of a dense network of disclination lines (*17*). The precise relationship if any, between icosahedral Al-Mn and the icosahedra in metallic glasses and the Frank-Kasper phases is another open question.

References and Notes

1. D. S. Shechtman *et al.*, *Phys. Rev. Lett.* **53**, 1951 (1984).
2. T. Komoda, *Jpn. J. Appl. Phys.* **7**, 27 (1968).
3. P. Chaudhari and D. Turnbull, *Science* **199**, 11 (1978).
4. K. F. Kelton and T. W. Wu, *Appl. Phys. Lett.* **46**, 1059 (1985).
5. R. D. Field and H. L. Fraser, *Mater. Sci. Eng.* **68**, L17 (1984–1985).
6. K. N. Knowles *et al.*, in preparation; D. Shechtman, D. Gratias, J. W. Cahn, *C. R. Acad. Sci. Ser. B*, in press.
7. R. Penrose, *Bull. Inst. Math. Appl.* **10**, 266 (1974); M. Gardner, *Sci. Am.* **236**, 110 (March 1977).
8. A. L. MacKay, *Physica* **114A**, 609 (1982); see also *Sov. Phys. Crystallogr.* **26**, 517 (1981).
9. R. Mosseri and J. F. Sadoc, in *Structure of Non-Crystalline Materials*, P. H. Gaskell, J. M. Parker, E. A. Davis, Eds. (Taylor and Francis, New York, 1983).
10. P. Kramer, *Acta Crystallogr. Sect. A* **38**, 257 (1982).
11. ______ and R. Neri, *ibid.* **40**, 580 (1984).
12. D. Levine and P. J. Steinhardt, *Phys. Rev. Lett.* **53**, 2477 (1984).
13. N. G. de Bruijn, *Ned. Akad. Weten. Proc. Ser. A* **43**, 39 (1981); *ibid.*, p. 53.
14. V. Elser, AT&T Bell Laboratories preprint; M. Duneau and A. Katz, Ecole Polytechnique, Palaiseau, preprint. See also D. Mercier and J. S. Levy [*Phys. Rev. B* **27**, 1292 (1983)] and P. A. Kalugin, A. Yu. Kitaer, and L. C. Levitor [*J. Exp. Theor. Phys.* **41**, 119 (1985)].
15. L. D. Landau, *The Collected Papers of L. D. Landau*, D. ter Haar, Ed. (Gordon and Breach–Pergamon, New York, 1965); G. Baym, H. A. Bethe, C. Pethick, *Nucl. Phys. A* **175**, 1165 (1971); S. Alexander and J. P. McTague, *Phys. Rev. Lett.* **41**, 702 (1978). The possibility of an icosahedral crystal is touched upon in the paper by Alexander and McTague.
16. P. Bak, *Phys. Rev. Lett.* **54**, 1517 (1985); *Phys. Rev. B*, in press.
17. D. R. Nelson and S. Sachdev, *Phys. Rev. B*, in press.
18. D. Levine *et al.*, *Phys. Rev. Lett.* **54**, 1520 (1985).
19. N. D. Mermin and S. M. Troian, *ibid.*, p. 1524.
20. G. S. Cargill, III, *Solid State Phys.* **30**, 227 (1975).
21. D. E. Moncton, J. D. Axe, F. J. DiSalvo, *Phys. Rev. Lett.* **34**, 734 (1975).
22. See, for example, J. Villain, in *Ordering in Strongly Fluctuating Condensed Matter Systems*, T. Riste, Ed. (Elsevier, New York, 1980).
23. L. M. Corliss, J. M. Hastings, R. J. Weiss, *Phys. Rev. Lett.* **46**, 1135 (1959); V. N. Bykov *et al.*, *Dokl. Akad. Nauk S.S.S.R.* **128**, 1153 (1959) [translation *Soviet Phys. Dokl.* **4**, 1070 (1960)].
24. D. R. Nelson and B. I. Halperin, *Phys. Rev. B* **19**, 2457 (1979).
25. R. Pindak *et al.*, *Phys. Rev. Lett.* **46**, 1135 (1981).
26. J. Budai, S. C. Davey, R. Pindak, D. E. Moncton, *Stanford Synchrotron Radiation Laboratory Report*, in press.
27. F. C. Frank, *Proc. R. Soc. London Ser. A* **215**, 43 (1952).
28. P. J. Steinhardt, D. R. Nelson, M. Ronchetti, *Phys. Rev. Lett.* **47**, 1297 (1981); *Phys. Rev. B* **28**, 784 (1983).
29. A typical translational correlation length, obtained from high-resolution x-ray scattering, is 300 Å [P. A. Bancel, P. A. Heiney, P. W. Stephens, A. I. Goldman, P. M. Horn, *Phys. Rev. Lett.* **54**, 2422 (1985)].
30. D. Shechtman, personal communication.
31. D. R. Nelson, *Phys. Rev. B* **28**, 5515 (1983).
32. S. Sachdev and D. R. Nelson, *Phys. Rev. Lett.* **53**, 1947 (1984).
33. We thank J. Cahn, H. Ehrenreich, V. Elser, C. Henley, P. Horn, M. Jaric, K. Kelton, S. Sachdev, F. Spaepen, P. Steinhardt, D. Turnbull, and M. Widom for helpful conversations. Supported by the National Science Foundation through the Harvard Materials Research Laboratory and by grant DMR-82-07431.

Neurotrophic Factors

Hans Thoenen and David Edgar

The development and maintenance of function of the nervous system results from the concerted interaction of a great variety of genetic and epigenetic regulatory mechanisms. Transplantation and ablation experiments performed during this century have demonstrated that the survival of developing vertebrate neurons can be determined by their fields of innervation (*1*). So far, however, only one trophic factor has been shown to be responsible for this epigenetic determination of neuronal survival: the protein nerve growth factor (NGF) was demonstrated to be required for the survival of developing peripheral sympathetic and sensory neurons by showing that neutralization of endogenous NGF by antibodies to NGF (anti-NGF) resulted in the death of these neurons (*2*). More recently, numerous tissue culture experiments have been used to show that NGF is only one of a number of molecules able to maintain the survival of embryonic neurons in vitro, implying that such molecules might also function as trophic factors to support neuronal survival in vivo (*3*). The central thesis of this article is that in order to prove that putative trophic factors (detected by experiments in vitro) do have a physiological role, it is necessary to purify them to produce specific antibodies to them. Accordingly, the consequences of neutralization of the endogenous molecules in vivo—and hence their physiological role—can then be established.

Nerve Growth Factor

The detection of large amounts of NGF in the submandibular gland of the male mouse some 30 years ago was a prerequisite for its purification, necessary for the production of anti-NGF to delineate the neurotrophic actions of NGF in vivo (*2*). In addition, determination of the amino acid sequence of mouse NGF more than a decade ago (*4*) provided the information necessary for its recent molecular cloning (*5*). This work has now led to the elucidation of the structure of the NGF precursor and its genomic organization. Thus, the major part of the precursor sequence has been shown to be on the amino terminal side of β-NGF (the active subunit of the NGF molecule), whereas the carboxyl terminal arginine is followed only by two amino acids. The region coding for β-NGF represents about one-third of the total precursor messenger RNA (mRNA). Analysis of the organization of mouse and human genomes has shown that the NGF gene is present as a single copy, and that all the information for the β-NGF sequence is located in a single exon. Moreover, the amino acid sequence homology of mouse and human NGF is more than 90 percent, as deduced from the genomic DNA sequence (*5*).

A sensitive two-site enzyme immunoassay allowing determination of the NGF present in effector organs has only recently been developed, allowing a major gap in the NGF story to be closed (*6*). These investigations demonstrated a correlation between the density of sympathetic innervation and the levels of NGF in the corresponding peripheral target tissues; experiments with tissue culture have shown that the local concentration of NGF determines the extent of ramification of sympathetic nerve fibers in vitro (*7*), implying that the levels of NGF in target tissues may be responsible for the density of sympathetic innervation. Tissue culture experiments have also shown that target tissues can synthesize NGF in vitro (*8*), and recent work with nucleic acid probes to quantify the mRNA for NGF demonstrates that levels of NGF are correlated with the amounts of its mRNA (*9*). Thus, the rate of synthesis of NGF in target tissues is probably determined by regulation of

---

Hans Thoenen and David Edgar are at the Department of Neurochemistry of the Max-Planck-Institute for Psychiatry, D-8033 Martinsried/Munich, Federal Republic of Germany.